Modification of excitation and charge transfer in cavity quantum-electrodynamical chemistry

Christian Schäfer[a,b,1], Michael Ruggenthaler[a,b], Heiko Appel[a,b], and Angel Rubio[a,b,1]

[a]Max Planck Institute for the Structure and Dynamics of Matter, 22761 Hamburg, Germany; and [b]The Center for Free-Electron Laser Science, 22761 Hamburg, Germany

Contributed by Angel Rubio, December 12, 2018 (sent for review August 16, 2018; reviewed by Victor S. Batista, Prineha Narang, and Vahid Sandoghdar)

Energy transfer in terms of excitation or charge is one of the most basic processes in nature, and understanding and controlling them is one of the major challenges of modern quantum chemistry. In this work, we highlight that these processes as well as other chemical properties can be drastically altered by modifying the vacuum fluctuations of the electromagnetic field in a cavity. By using a real-space formulation from first principles that keeps all of the electronic degrees of freedom in the model explicit and simulates changes in the environment by an effective photon mode, we can easily connect to well-known quantum-chemical results such as Dexter charge-transfer and Förster excitation-transfer reactions, taking into account the often-disregarded Coulomb and self-polarization interaction. We find that the photonic degrees of freedom introduce extra electron–electron correlations over large distances and that the coupling to the cavity can drastically alter the characteristic charge-transfer behavior and even selectively improve the efficiency. For excitation transfer, we find that the cavity renders the transfer more efficient, essentially distance-independent, and further different configurations of highest efficiency depending on the coherence times. For strong decoherence (short coherence times), the cavity frequency should be in between the isolated excitations of the donor and acceptor, while for weak decoherence (long coherence times), the cavity should enhance a mode that is close to resonance with either donor or acceptor. Our results highlight that changing the photonic environment can redefine chemical processes, rendering polaritonic chemistry a promising approach toward the control of chemical reactions.

QED chemistry | correlated chemistry | long-range energy transfer | strong light–matter interaction | cavity QED

One of the basic questions of chemistry is how different constituents such as electrons and atoms form new structures, which have properties distinct from the individual constituents, and how these structures can undergo further chemical reactions. Such reactions, which are traditionally investigated and controlled by, e.g., catalytic surfaces, modification of solvents, pressure, or heat and irradiation, are determined to a large extent by energy or charge transfer between subsystems. For instance, a donor molecule (D) can transfer charge or excitation energy to an acceptor molecule (A) (Fig. 1), which can then lead to structural changes.

Only recently, mainly driven by experimental results (1), the influence of individual photons in the form of vacuum fluctuations of the electromagnetic field on structures and chemical reactions has become the focus of intense research (2). By changing the environment and with this the photon field, e.g., by an optical cavity, these seemingly tiny modifications that are not captured by traditional quantum mechanics can have a strong influence (3–7). This alternative way to investigate and control chemical properties has the appealing features that it seems to be robust, even for room temperature and ambient conditions, and that it does not need an external energy source, such as a laser field, that could lead to ionization or heating of the system under investigation. Theoretically, the interplay of individual photons with chemical structures and reactions is considered, usually with quantum-optical models. These models use a very restricted representation of the matter subsystem (atoms and molecules) of only a few levels and then couple it to the mode of an optical cavity (5, 8, 9). The complex environment of the few-level system coupled to one mode is then often subsumed in an effective bath. This simplified treatment, which makes the determination of real-space and correlation observables very challenging, is in stark contrast to the usual first-principle treatment of systems in quantum chemistry. In this case, the complex interplay between the matter degrees of freedom in real space are responsible for detailed structures and reactions.

In this work, we identify fundamental changes in chemical properties and reactivities due to coupling to the vacuum of a cavity when we treat the matter subsystem from first principles in real space. We show that well-known quantum-chemical effects, such as Dexter charge-transfer probabilities, can be strongly modified in a controlled manner. This highlights that photons (even only those originating from quantum vacuum fluctuations) allow for a promising control knob of chemical reactions, also in real space. Furthermore, we find effects due to a strong coupling of light and matter that cannot be captured by simplified few-level models.

As a first example, we consider how a photon mode induces correlations also between matter subsystems and entangles them over large distances. This leads to, among others, an earlier onset of the static-correlation limit, where A and D are well described by a minimal linear combination of atomic orbitals (LCAO).

Significance

Excitation and charge transfer are fundamental processes in nature, and controlling these processes is a major goal of quantum chemistry. While these processes are well understood for the usual free-space case, when the electromagnetic vacuum is changed due to, e.g., a cavity, these processes can be dramatically different. We consider these changes in transfer processes with real-space donor–acceptor models, where we put an emphasis on the impact of electron–electron correlations. We find results in line with recent experiments, where strong light–matter interaction leads to enhanced transfer reactions, even when in the corresponding free-space situation no transfer should be possible. We highlight that the processes depend crucially on the Coulomb and self-polarization interactions.

Author contributions: C.S. and A.R. designed research; C.S., M.R., H.A., and A.R. performed research; C.S., M.R., H.A., and A.R. analyzed data; and C.S., M.R., H.A., and A.R. wrote the paper.

Reviewers: V.S.B., Yale University; P.N., Harvard University; and V.S., Max Planck Institute for the Science of Light.

Conflict of interest statement: A.R. and V.S. are both members of the QuantERA RouTe consortium. They are not currently collaborating.

[1]To whom correspondence may be addressed. Email: angel.rubio@mpsd.mpg.de or christian.schaefer@mpsd.mpg.de.

This article contains supporting information online at www.pnas.org/lookup/suppl/doi:10.1073/pnas.1814178116/-/DCSupplemental.

Published online February 7, 2019.

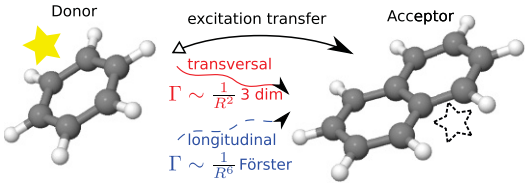

Fig. 1. Schematic illustration of typical excitation transfer in free space between donor and acceptor, which consists of transversal (radiative) and longitudinal (nonradiative, Förster) contributions. Here, R is the distance between donor and acceptor. If the electromagnetic vacuum is changed due to, e.g., an optical cavity, especially the transversal contribution is expected to differ from its free-space form, therefore deviating from the geometric dilution $1/R^2$ behavior in three dimensions.

Together with the following investigations, this illustrates possibilities to use cavities and their photons to investigate directly matter–matter correlations.

Next, to contrast to well-known results from quantum mechanics in real space, we then investigate changes in charge-transfer (Dexter) and excitation-transfer (Förster) reactions for a donor–acceptor system. In quantum mechanics, charge transfer is understood perturbatively by considering the overlap of exponentially decaying wave functions. In this case, indeed, electronic charge density moves from D to A. As a consequence, with increasing distance between the two components, the exponential decaying overlap leads to an exponentially decaying charge-transfer probability $\Gamma \sim \exp(-(I_A + I_D)|\mathbf{R}_A - \mathbf{R}_D|)$, where $I_{A/D}$ and $\mathbf{R}_{A/D}$ are the corresponding ionization potentials and (mean) positions, respectively. This perturbative limit of Dexter charge transfer dominates typically length scales of a few to tens of Angstroms depending on its participants (10). Here, we show how the coupling to a cavity can change this well-known behavior and allows, by increasing the distance between A and D, to even invert the charge transfer—i.e., charge flows from A to D.

Excitation energy transfer, on the other hand, does not demand a transfer of charge, but is mediated by transversal (observable/real) and longitudinal (Coulomb) photons as illustrated in Fig. 1. In free space, the transfer rate decreases with $1/|\mathbf{R}_A - \mathbf{R}_D|^2$ due to geometric dilution, dominating the far-field rate. The Coulombic participation, typically referred to as Förster excitation energy transfer, can be approximated as a dipole–dipole interaction after a certain spatial separation and is decaying as $\Gamma \sim 1/|\mathbf{R}_A - \mathbf{R}_D|^6$, dominating typically the near-field beyond the Dexter domain up to 30 nm (11).

If we couple A and D to a cavity, the characteristic transversal contribution changes. Its efficiency depends strongly on the intrinsic coherence time of the coupled system, and we identify two major domains. For strongly decoherent systems (short coherence times), a cavity that has a frequency in between the isolated resonances of A and D shows the highest excitation-transfer efficiency. For long-time coherent systems, we find that the highest efficiency is provided if the cavity is in resonance with the isolated D or A resonances. Furthermore, we find that the usually discarded dipole self-polarization term has a large influence on the dynamics of the combined light–matter system, especially for strong-coupling situations. Finally, we highlight that, even for the coupled system, it is the electron–electron correlation that dominates the excitation transfer.

This paper is structured as follows: First, the theoretical setting is explained in Theoretical Framework. We then consider the influence of matter–photon correlations on the equilibrium structure in Equilibrium Long-Range Correlation, before we investigate charge transfer in Charge Transfer. Next, we discuss excitation energy transfer in Excitation Energy Transfer and then highlight the influence of matter–matter correlations in Photon-Induced Correlations. Finally, we present the conclusions of our work and provide a perspective outlook in Summary and Conclusion.

Theoretical Framework

We focus on changes of the electronic properties (which drive the aforementioned energy-transfer processes) due to coupling to the photon vacuum and, hence, keep photonic as well as all electronic degrees of freedom explicit. We include the effects of the nuclei in the Born–Oppenheimer approximation—i.e., we consider the electronic wave function as a conditional wave function of the nuclear positions.* Furthermore, following the highly successful approach of quantum chemistry, we take the photon bath of the bare electromagnetic vacuum into account by renormalizing the bare masses of the charged particles and use their respective physical values (13). Instead of performing a renormalization of the masses to new values that take into account the changes in the vacuum, we simulate these changes by explicitly keeping one of the enhanced modes due to a cavity. This allows us to recover the well-known matter Hamiltonian when we let the coupling to this mode go to zero. While this simplified treatment of dissipation is expected to be accurate for static (eigenfunction) calculations, in the time-dependent case, this simplified treatment will lead to wrong long-time dynamics. For long-time dynamics, the influence of the photon and phonon bath (that we disregarded due to the Born–Oppenheimer and zero-temperature approximation) will become essential. The latter one will become increasingly important, already in equilibrium at finite temperature, leading to a thermal occupation of phononic eigenstates on the energy-scale $k_B T$. We take this into account effectively by introducing relevant coherence times—i.e., we consider coherent dynamics up to a finite time T, after which we assume that the bath will damp the dynamics. The coherence time is usually determined by the coupling to the phonon modes, which is typically between a few tens up to hundreds of femtoseconds in, e.g., light-harvesting complexes (14, 15). For such short-time dynamics, the decoherence due to photon loss (typically on the order of picoseconds) is indeed a minor contribution.

As a minimal example of the above description, we consider a one-dimensional dimer model coupled to one effective photon mode. The polarization of the effective mode is therefore in the direction of the one-dimensional model. We assume the validity of the long-wavelength approximation—i.e., since the wavelength of the photonic mode is much larger (hundreds of nanometers) than the extension of the molecular system (few Angstroms), we can disregard the inhomogeneity of the electromagnetic field to determine the electronic properties (2, 16). In this case, the Hamiltonian in SI units is given by

$$\begin{aligned}\hat{H}(t) = &-\sum\nolimits_{n=1}^{2} \frac{\hbar^2}{2m_e}\nabla_{x_n}^2 - \frac{e^2}{4\pi\varepsilon_0}\sum\nolimits_{n,j=1}^{2} \frac{Z_j}{\sqrt{(\hat{x}_n - R_j)^2 + 1}} \\ &+ \frac{\xi(t)}{4\pi\varepsilon_0}\frac{e^2}{\sqrt{(\hat{x}_1 - \hat{x}_2)^2 + 1}} + \hbar\omega\hat{a}^\dagger\hat{a} \\ &+ \frac{1}{2}(\lambda(t)\hat{X})^2 - \sqrt{\frac{\hbar\omega}{2}}\lambda(t)\hat{X}\left(\hat{a}^\dagger + \hat{a}\right),\end{aligned}$$

with the electronic dipole operator $\hat{X} = -|e|\,[\hat{x}_1 + \hat{x}_2]$. Here, the physical mass m_e already contains the effect of the continuum of all modes other than the one enhanced by the cavity. To find the proper physical transfer behavior, it is essential that the longitudinal interaction and nuclear potentials (at the positions

*The here-applied description can be extended to account for the full quantum behavior of nuclei, electrons, and photons following, e.g., refs. 2 and 12.

of the nuclei $R_{1/2}$) resemble the correct $1/r$ form, also in one dimension. We therefore use the widely applied soft-Coulomb approximation. The nuclei have the effective charge $Z_{1/2}$, and we have a coefficient $\xi(t) \in [0,1]$ that allows us to quench the system by switching on the Coulombic interaction term. The electron–photon coupling for a mode with frequency ω is deduced from the nonrelativistic limit of the Hamiltonian of quantum electrodynamics (QED) (2, 13, 17) and reads as (16)

$$\hat{H}_{ep} = \frac{1}{2}\left[\hat{p}^2 + \omega^2\left(\hat{q} - \frac{\lambda}{\omega}\cdot\hat{X}\right)^2\right],$$

with the displacement coordinates $\hat{q} = \sqrt{\frac{\hbar}{2\omega}}(\hat{a} + \hat{a}^\dagger)$ and $\hat{p} = \sqrt{\frac{\hbar\omega}{2}}i(\hat{a}^\dagger - \hat{a})$, as well as the coupling $\lambda = \sqrt{1/\varepsilon_0 V}$ that determines the transversal light–matter interaction between electronic system and cavity with effective mode volume V. In the following, the coupling is given via the unitless relation between coupling-strength $g = ea_0\sqrt{\frac{\hbar\omega}{2}}\lambda$ and relevant energy-scale $\hbar\omega$, such that $g/\hbar\omega$ characterizes the strength of the light–matter interaction in relation to the matter excitations (16, 17). Similar to the longitudinal interaction, which is due to the exchange of longitudinal photons (2, 13, 17), also the transversal interaction can be switched on and off. This time, however, different values for nonzero $\lambda(t)$ will be used depending on whether we want to investigate weak or strong coupling situations.[†] By weak, we mean that the electronic structure is almost identical to the free-space case ($\lambda = g = 0$), and the Rabi splitting, if the cavity is in resonance with an electronic transition, is very small. By strong, we mean that the electronic structure changes considerably, and, if in resonance, also the Rabi splitting is large.

In the following, we consider two different realizations of the above dimer model. Setup 1 (described in Fig. 2) is a hydrogen-like dimer, where D has a slightly higher nuclear charge of $Z_D = 1.2$ in relation to A with $Z_A = 1$. Setup 2 (illustrated as well in Fig. 2) has excitation energies close to experimental values of $2-3\ eV$, mimicking the energetic structure of cyanine dyes (5), with nuclear charges $Z_A = 2/9$ and $Z_D = (2+1/5)/9$. We denote the corresponding single-electron states by $\{\phi_0^A, \phi_1^A\}$ and $\{\phi_0^D, \phi_1^D\}$. Furthermore, in situations where we refer to "isolated" constituents (in Excitation Energy Transfer), we specifically mean that D and A are solved independently with only one electron but still individually coupled to the cavity—i.e., $g \neq 0$. Put differently, we solve the single-electron D or A problem coupled to the cavity. This allows us to discuss the relations between the individual polaritons of D and A and the many-body states of the coupled light–matter system.

The numerical calculations are performed with a real-space grid of variable length, and the photon mode is expanded in Fock-number states. This means that the combined electron–photon Hilbert space consists of $101^2 \cdot N_{pt}$ to $301^2 \cdot N_{pt}$ states. Consequently, the enormous amount of degrees of freedom in the electron–photon system accounts for decoherence on attosecond time scales. More details are given below the figures and in the *Materials and Methods*.

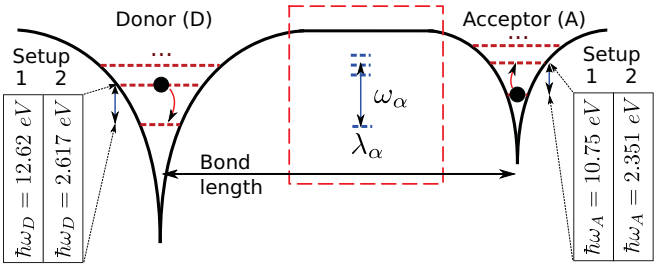

Fig. 2. Setup 1 and 2 of the two-electron dimer model with variable bond length, Coulomb, and cavity interactions. The lowest single-electron excitation of D is $\hbar\omega_D = 12.62\ eV$ or $\hbar\omega_D = 2.617\ eV$, and the lowest single-electron excitation of A is $\hbar\omega_A = 10.75\ eV$ or $\hbar\omega_A = 2.351\ eV$ for setup 1 or 2, respectively.

Equilibrium Long-Range Correlation

Let us start by analyzing the influence of the changed photonic vacuum on the equilibrium of the model dimer. The ground state, also for open systems, can be influenced by a change in the photonic bath (13, 18, 19), which we take into account by one effective photon mode (see *SI Appendix*, section 1 for more information). The rest of the photon bath is subsumed, as is usually done, in the physical mass of the electrons. To harness the possibilities of our real-space formulation, we will consider the influence of the extra photonic degrees of freedom on the dissociation of our model dimer, where for each bond length or interatomic distance $|R_A - R_D|$ in our model system 1 (Fig. 2), we get a different Born–Oppenheimer problem that we can investigate.

For $g = 0$, this problem has two well-known limiting cases: For very small bond lengths, the electronic system can be accurately reproduced by a single Slater determinant, and the influence of additional Slater determinants (correlation) decreases exponentially fast. In this domain, Hartree–Fock and simple density-functional approximations perform adequately. For very large bond lengths (the atomistic limit), the electrons become equally distributed on both components while remaining fully antisymmetrized. As a consequence, the wave function is well represented by a linear combination of two determinants that are due to symmetric and antisymmetric combinations of two local atomic orbitals—i.e., a minimal LCAO of gerade and ungerade states $\{\varphi_g, \varphi_u\}$. For this (spin-singlet) ground state the electronic one-body reduced-density matrix (1RDM)

$$\gamma_e(x_1, x_1') = \int dx_2 \Psi(x_1, x_2)\Psi^*(x_1', x_2),$$

which can be diagonalized by the so-called natural orbitals (NOs) $\varphi_k(x)$ and natural occupations n_k as

$$\gamma_e(x_1, x_1') = \sum_{k=1}^{\infty} n_k \varphi_k(x_1)\varphi_k^*(x_1'),$$

then becomes specifically simple—i.e., $\gamma_e(x_1, x_1') \approx \frac{1}{2}(\varphi_g(x_1)\varphi_g^*(x_1') + \varphi_u(x_1)\varphi_u^*(x_1'))$—and all other NOs are exponentially suppressed (Fig. 3). Note that, in contrast to the usual case, we have chosen to normalize the 1RDM to one. This allows us to draw a simple connection to the notion of a pure density matrix, since even though the 1RDM is specifically simple in structure, it has in this case still a purity smaller than one—i.e., $tr(\gamma_e^2) \approx \sum_{k=1}^{\infty} n_k^2 < 1$. Any occupation beyond a single NO is in the present context often called static correlation, which is equivalent to a nonzero generalized concurrence (20). However, in the Coulombic case, we cannot make the static correlation any

[†]While here we just adopt the coupling strength by hand, in an experiment there are several ways to do so. One either really makes the volume of the cavity smaller, which would demand an effective mode-length L between 67 and 5.7 Å to reach the applied light-matter interactions (leading into the domain of nanoplasmonics or circuit QED), increases the reflectivity of the mirrors or increases the number of molecules such as done in polaritonic chemistry. While, e.g., nanoplasmonics allows for single-molecule couplings on scales close to values presented in this work, so far, the loss rates are relatively high. Increasing the numbers of molecules has two contributions (16): an increase of excitations (number of photons) of the electromagnetic field (coupling to individual molecules) and a collective enhancement (coupling to the ensemble of molecules). Here, we focus on local changes of the molecular systems and comment on possible collective modifications in *Summary and Conclusion*.

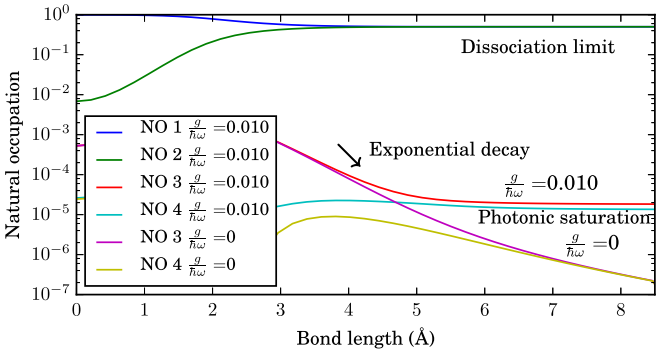

Fig. 3. Natural occupations of $\gamma_{e,p}$ with and without photonic coupling for frequency $\hbar\omega = 12.62$ *eV*. While for the uncoupled systems, the higher-lying NOs, e.g., 3 (purple) and 4 (yellow), are exponentially suppressed with bond length, and the dark cavity introduces explicit electron–electron correlation that become distance-independent. In the atomistic limit, the cavity therefore introduces static correlations beyond the usual Coulomb case. The simulation box is 26.5 Å, with a spacing of 0.0529 Å and 10 photon number states.

larger. Even if we increased the longitudinal interaction, in the atomistic limit, we would still only have two occupied NOs.

Next, we couple this system to a photonic mode (details are given in Fig. 3). Again, we want to consider the static correlation, but since we now also have the photon mode, we consider a slight extension of the 1RDM to the photonic case by

$$\gamma_{e,p}(x_1\, q, x_1'\, q') = \int dx_2 \Psi(x_1, x_2, q)\Psi^*(x_1', x_2, q').$$

If we accordingly extend also the definition of the NOs to include the photon coordinate, we find $\gamma_{e,p}(x_1\, q, x_1'\, q') = \sum_{k=1}^{\infty} n_k \varphi_k(x_1\, q)\varphi_k^*(x_1'\, q')$. If we would integrate out also the photon coordinate, we could get static correlation, even for situations where there is no true electronic correlation.[‡] If we find occupation numbers that are different from the above LCAO case, then we have influenced the genuine static electron–electron correlations of the system.

Indeed, in Fig. 3 we see that, already for small bond lengths, the coupled and uncoupled cases are different. The photon mode makes the single-Slater-determinant ansatz less accurate—i.e., the higher-lying NOs have a larger occupation. These differences become more pronounced as we approach the atomistic limit—i.e., for large bond lengths. While both cases have dominant occupations of the two first NOs, in the coupled case, the higher-lying NOs are no longer exponentially suppressed, but saturate and become distance-independent. Thus, in the atomistic limit, we have more than only two NOs occupied and, hence, have larger static correlations. Physically, this is to be expected, since as long as the dipole approximation is valid, the photon field interacts with both electrons simultaneously, independently of their distance. That also means that there is a tiny bond energy, even over very large distances, due to the photons shared by the two electrons.

Furthermore, the cavity-induced correlation results in a slightly earlier onset of the static-correlation limit. This happens because the photonic interaction tends to localize charge densities stronger—i.e., for realistic light–matter couplings, it reduces local polarizations. As a consequence, bound molecules tend to reduce their bond length (also observed in ref. 18) due to an accumulation of charge between the molecules, while separated charges accumulate at their local molecules [also observed in theoretical calculations for realistic molecules (21)]. This effect, however, is rather small in relation to effects discussed in the following sections. The major difference is that in equilibrium without external perturbations, all of the effects are purely due to quantum fluctuations, and the (expectation values of the) electromagnetic fields are zero. In the following sections, where the dynamics of the electrons also generate nonzero electromagnetic fields, the classical part of the photon field can enhance effects. But we will see in Excitation Energy Transfer that photon-assisted electron–electron correlations still play a major role in molecular dynamical processes.

Charge Transfer

Let us next move on to dynamical processes where energy is transferred between two subsystems. We first investigate the influence of the photon field on charge-transfer processes. We consider setup 1, presented in Fig. 2, and take as the initial state an eigenstate of the coupled Hamiltonian that has most of its charge density on D. Then, we perturb this eigenstate weakly with an external pulse $|e|\hat{x}E_0\delta(t-t_0)$, $t_0 = 0.12$ fs, where the delta peak was numerically represented by a sharp Lorentzian with width $\sigma = 10^{-4}$ fs, triggering a broad spectral evolution as commonly done for response calculations, and the origin of the coordinate system is located between A and D. From the dynamics of the system, we investigate the induced charge-transfer process (see *SI Appendix*, section 2 for details on an alternative approach). We apply here a positive field $E_0 = 0.144\frac{eV}{e\cdot\text{Å}}$, which leads to an almost pure charge transfer from D to A.[§] We then measure the efficiency by dividing the system into two parts—one to the left of $x = 0$ (associated with D) and the other to the right (associated with A)—and then define the total charge transfer (leaving D toward A)

$$c(t) = \int_0^t dt' \int_0^\infty dx[n(x, t') - n(x, 0)],$$

and the maximal time-resolved transfer

$$c^{max}(T) = max_{t\in T}[|c(t)|],$$

for a fixed coherence time $T = 10$ fs, while keeping track of the sign of $c(t_{max})$.[¶] We then repeat this for different interatomic distances $R_{AD} = |R_A - R_D|$.

The pure Coulombic system ($\xi = 1$ and $g = 0$) has two different domains. The first one is the molecular domain (below the interatomic distance of 5 Å; see also Fig. 3), where we have significant electronic delocalization and charge is transferred quickly, oscillating multiple times forward and backward with small amplitudes such that the effective transfer averages to almost zero. More interesting is the second domain shown in Fig. 4*A* starting at ∼5 Å. For this interatomic distance, the efficiency to transfer charge from D to A is maximal, and beyond this point, we observe decay with exponential character over the interatomic distance (note especially the blue curve with

[‡]For instance, if we have only one electron coupled to a mode then while the extended 1RDM ($\gamma_{e,p}$) would have only one nonvanishing occupation, the reduced (γ_e) would have more than one, simply as a consequence of that the correlated state cannot be factorized. Furthermore, since the electrons and photons were uncoupled in the previous case, it is easy to extend it to the present situations by just multiplying with the bare photonic vacuum. This does not affect the occupation numbers.

[§]The results are invariant under inversion of the kick, i.e., whether we consider the transfer from D to A or the inverse process from A to D by inverting the kick $E_0 \to -E_0$.

[¶]While our results depend quantitatively on the integration time T, qualitatively, also indicated by higher amplitudes at the resonances, our results are consistent for different T. For the energies present in this setup, 10 *fs* relates to a medium to high coherence. The maximum time-resolved transfer observable is less dependent on the chosen integration time.

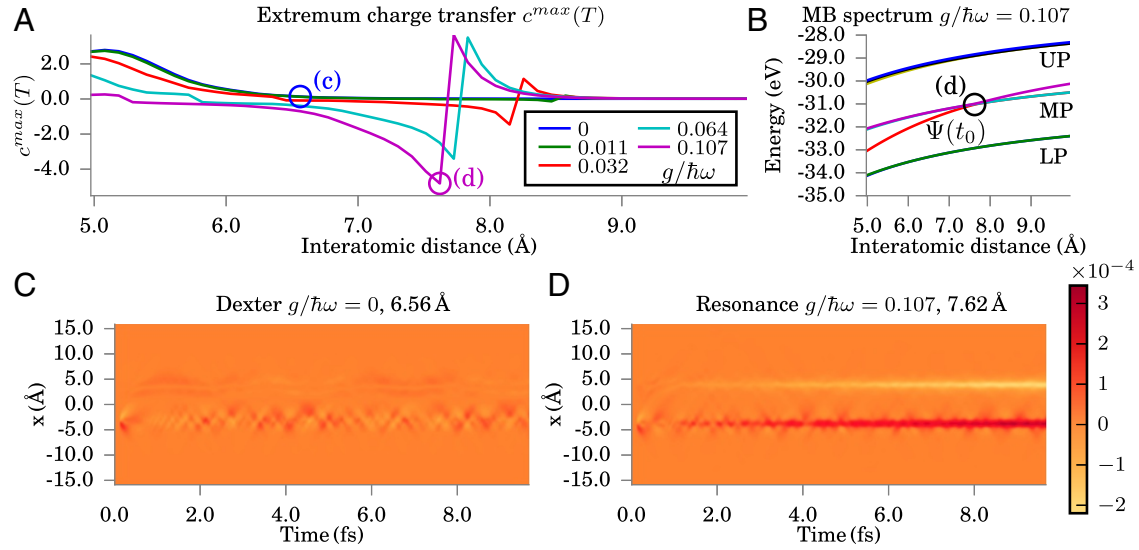

Fig. 4. (*A*) The integrated charge transfer as a function of the interatomic distance for different light–matter couplings ($\xi = 1$ and $\hbar\omega = 11.97$ *eV*). The increasing localization of charge with increasing coupling shifts the domain of Dexter-type exponential decay to smaller distances with increasing coupling. New (inverse) maxima of charge transfer arise, and they are connected to avoided crossings of the initial many-body eigenstate with polariton many-body (MB) eigenstates in *B*. In *C* and *D*, we show the charge dynamics of Dexter-type and resonant light–matter-originated transfer in terms of the time-dependent density-difference $n(x, t) - n(x, 0)$ for the indicated interatomic distances. The simulation box is 31.84 Å, with a spacing of 0.1058 Å and 30 photon number states.

$g/\hbar\omega = 0$). This exponential decay corresponds to Dexter charge transfer; see Fig. 4*C* for a representative example.[#]

Next, we switch on the coupling to the photon field. We vary the light–matter coupling and select a frequency in between the single-electron first excitation of D and A, respectively (details are given in Fig. 4). We again change the interatomic distance and observe a drastically different behavior. While the strong light–matter interaction bleaches the previously optimal Dexter transfer, we find around 8 Å resonances with optimal charge transfer (see Fig. 4*D* for the electronic dynamics) which feature a drastic amplification of efficiency in relation to the pure Coulomb system. We again observe an exponential behavior around the resonance which features a sudden inversion of the transfer characteristic—i.e., while the light–matter interaction now inverts the transfer (A to D instead of D to A) for interatomic distances smaller than the resonance, it suddenly switches into a very efficient transfer from D to A for increasing distances and is exponentially suppressed for even larger distances. This violation of the usual Dexter behavior can be understood physically from the many-body energies of the coupled matter–photon system (Fig. 4*B*). Stretching the molecule increases the dipole and lets the initial state change its energetic position in relation to other states. At specific distances, the initial state with almost all charge on D then shows an avoided crossing with the spin-singlet middle (and in principle also other) polariton many-body eigenstate, undergoes a small but sudden decrease in the total dipole, and, depending on the character of these states, one can find an efficient (resonant) transfer from D to A, or A to D. With increasing light–matter interaction, the contribution of D and A to the middle polariton increases (see, e.g., Fig. 9) and consequentially amplifies the efficiency close to the resonance, while the competing Coulomb-mediated transfer is shifted toward smaller interatomic distances. Therefore, by adjusting frequency or coupling of the cavity, we can control the position of these many-body resonances such that the charge transfer can be controlled. Taken together with experimental demonstrations of cavity-controlled chemical reactions (see, e.g., ref. 4), this highlights the feasibility of steering electronic quantum dynamics by controlling the electromagnetic vacuum. The extension beyond few-level descriptions further enables a fully consistent treatment of chemistry and light–matter-induced effects—e.g., changes in transition states, chemical reactions, and common observables.

Excitation Energy Transfer

Next, we consider the transfer of excitation energy. Here, we investigate setup 2[‖] as presented in Fig. 2, which has energies that are comparable to recent experimental studies, where a cavity has proven to allow excitation energy transfer over distances of hundreds of nanometers (5, 6), going far beyond the typical limit of tens of nanometers in Förster energy transfer. The initial state is chosen to be the spatially symmetric (spin singlet) product of the single-electron ground state of A and the single-electron first-excited state of D, as well as the bare photonic vacuum,

$$\text{i.e.,}\quad |\psi(0)\rangle = \sqrt{1/2}(|\phi_0^{\mathrm{A}}\rangle \otimes |\phi_1^{\mathrm{D}}\rangle + |\phi_1^{\mathrm{D}}\rangle \otimes |\phi_0^{\mathrm{A}}\rangle) \otimes |0\rangle_{\mathrm{p}}.$$

After quenching the Hamiltonian—i.e., this assumes that the system reacts slower than the conditions change—the initial state is no longer an eigenstate of the coupled system and starts to evolve. To monitor the excitation-energy-transfer process, we evaluate the projection of the evolved state on the first-excited transfer target state

$$|\psi_1(0)\rangle = \sqrt{1/2}(|\phi_1^{\mathrm{A}}\rangle \otimes |\phi_0^{\mathrm{D}}\rangle + |\phi_0^{\mathrm{D}}\rangle \otimes |\phi_1^{\mathrm{A}}\rangle) \otimes \hat{\mathbb{1}},$$

and denote

$$e_1(t) = |\langle\psi_1(0)|\Psi(t)\rangle|^2, \qquad [1]$$

[#]We note here that the exponential suppression of charge transfer can also be inferred from the exponential suppression of higher-order NOs in Fig. 3. For large interatomic distances, it is only the single-electron D and A orbitals that form $\{\varphi_{\mathrm{g}}, \varphi_{\mathrm{u}}\}$ that determine the perturbative picture of the Dexter transfer. From before, we can therefore already expect that the change in the NO occupations will have some influence on the charge-transfer dynamics.

[‖]To avoid that our observations are limited to a special configuration, we selectively performed reference calculations using our previous setup 1. Those are qualitatively in line with the following results. Note that different energy scales result accordingly in adjusted couplings and time frames.

the first-order or linear excitation energy transfer. Here, first-order/linear corresponds to the fact that we exchange the lowest-order excitation from D to A and that this excitation energy transfer would be dominant in the linear-response regime. From this, we can define the integrated first-order excitation energy transfer

$$E_1(T) = \int_0^T dt\ e_1(t), \qquad [2]$$

where the upper limit T is the chosen coherence time—i.e., small T (of the order of a few femtoseconds) indicates that the discarded bath leads to a fast decay of coherence. By exchanging the first-excited state with the second-excited state—i.e., $\phi_1^A \rightarrow \phi_2^A$—we can accordingly define a second-order or nonlinear excitation transfer $e_2(t)$ and integrated second-order excitation transfer $E_2(T)$.

Distance Dependence of Excitation Energy Transfer. Let us focus first on the distance dependence of the excitation energy transfer. If we choose a long coherence time of $T = 60.5$ fs and then plot the resulting integrated first-order excitation energy transfer for different interatomic distances in Fig. 5, we find for the purely Coulombic case that the longitudinal transfer decays as expected and resembles the usual $1/|R_1 - R_2|^6$ Förster behavior. In the coupled case (see Fig. 5 for details), the transversal light–matter coupling is strongly enhancing the excitation energy transfer (note the factor of 400 in Fig. 5), and for larger interatomic distances, the efficiency is even slightly increasing after an initial decay, with a tendency to saturate once the Coulombic near-field effects vanish. This is in stark contrast to the usual Förster behavior. Thus, increasing the coupling strength amplifies the transfer drastically, dominating the longitudinal interaction, even for small distances, and leading to an almost distance-independent transfer efficiency for large interatomic distances. This finding is in agreement with recent experiments (5).

However, it is important to note that with increasing light–matter coupling, the excitation-transfer process strongly depends on the self-polarization dipole–dipole interaction (16, 21, 22) $(\lambda \cdot \hat{X})^2 = e^2 \sum_{n=1}^{2} (\lambda \hat{x}_n)^2 + 2e^2 (\lambda \hat{x}_1)(\lambda \hat{x}_2)$, which is often disregarded in quantum-optical models of excitation transfer. For weak coupling, this contribution, which for free-space situations approximately cancels with the longitudinal interaction after a certain distance (23), only slightly influences the excitation energy transfer (Fig. 6). Hence, in such cases, the self-polarization term would only become visible if we propagate

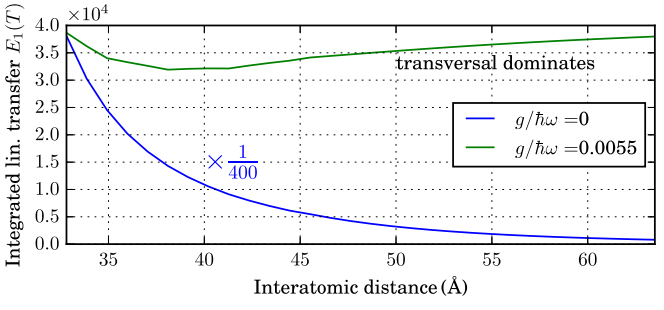

Fig. 5. Integrated first-order excitation energy transfer $E_1(T)$ for $T = 60.5$ fs for different interatomic distances. The Coulombic case (blue) decays as expected and is multiplied by a factor of 400 here to present the otherwise vanishingly small purely longitudinal transfer. The coupled case (green) with $g/\hbar\omega = 0.0055$ and $\hbar\omega = 2.612$ *eV* shows a drastic enhancement of the excitation energy transfer and is mostly distance-independent. The simulation box is 79.75 Å, with a spacing of 0.397 Å up to a interatomic distance of 44.45 Å, and 106.3 Å, with a spacing of 0.529 Å for interatomic distances >44.45 Å. We use six photon number states.

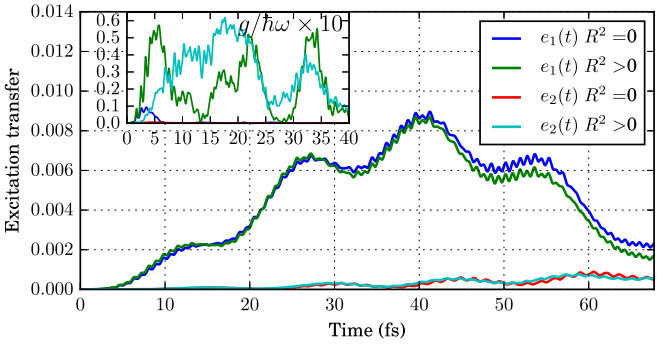

Fig. 6. First- and second-order excitation energy transfer with and without the self-polarization contribution R^2 with frequency $\hbar\omega = 2.340$ *eV* and interatomic distance 42.3 Å. For weak light–matter coupling $g/\hbar\omega = 0.0058$ (main plot), small differences are visible. For longer times, these small changes accumulate and lead to substantial differences, even for weak coupling (see also Fig. 10). For strong coupling (*Inset*; $g/\hbar\omega = 0.0579$) the differences are substantial already for short propagation times. This effect is not restricted to a resonant frequency but persists also off resonance. We further note that also the mode occupation changes drastically, e.g., for $g/\hbar\omega = 0.0579$ from ≈ 45 without to ≈ 1 with self-polarization. This originates from a strong charge displacement that appears for short times only without the self-polarization contribution, and, in contrast to other calculations in this section, the charge transfer dominates then the energy transfer. The simulation box is 79.75 Å, with a spacing of 0.397 Å and 100 photon number states, except for $g/\hbar\omega = 0.0579$ without self-polarization, where we used 250 photon number states.

for a long time. Put differently, if the coherence times are large. For strong coupling, however, this term leads to substantial differences already for very short times. This shows that the self-polarization term, which has been proven to be essential in the equilibrium, especially the ground state (16, 21, 22), also can have a strong influence on dynamical processes such as excitation-transfer reactions, especially for higher-order excitations.

Resonances and Efficiency. While we feature that light–matter coupling can lead to an efficient long-range excitation energy transfer, which is very distinct to the usual longitudinal Förster transfer, we would also expect that the efficiency can be enhanced resonantly for specific frequencies and couplings. The isolated energies of D and A coupled independently to the cavity (see discussion in Theoretical Framework) show the well-known Rabi splitting (see Fig. 7 for details).

As we couple D and A by the Coulomb interaction—i.e., $\xi = 1$—and also together to the cavity, the independent electron–photon states (lower and upper polariton for D and A, respectively) interact and build lower, upper, and middle polariton states. These states consist dominantly of a single excitation on D or A and the many-body ground-state plus a photonic excitation. The creation of such new light–matter-correlated states was not only observed in dilute gases (5), but also in extended systems (24) and circuit structures (25).

The assumption of a resonance that emerges from crossings of isolated polaritons—that is, shifting the lower D polariton into resonance with the upper A polariton—is in this case a too-drastic simplification, as can be seen from Fig. 7. This can only hold if A and D have drastically different numbers of particles, such that the effective coupling is different and the effective collective bright polariton state of one constituent is shifted stronger (7). However, the lack of such a simplified crossing picture does not exclude a resonance or most-favorable setup. Indeed, we will see in the following that the definition of such an optimal setup depends on the time scales that we are interested in and with this the given coherence times.

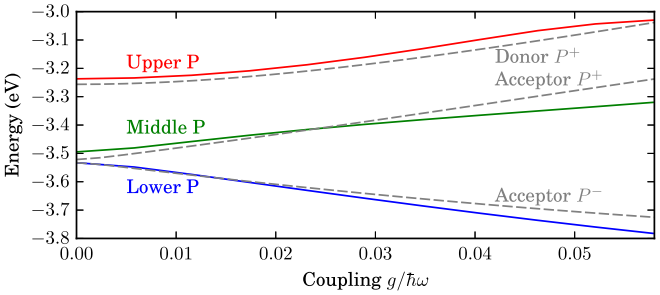

Fig. 7. The isolated A and D lower and upper polariton energies (dotted lines) and the fully interacting many-body system lower, middle, and upper polariton energies (thick lines) calculated for different coupling strengths. The frequency of the cavity $\hbar\omega = 2.340$ *eV* is close to resonance with the lowest single-electron excitation of A, and we have chosen an interatomic distance of 21.2 Å. We shifted the isolated energies by the ground-state energy difference $E_0^{g=0} - \varepsilon_0^A - \varepsilon_0^D = 0.367$ *eV* between correlated and isolated systems. Although the isolated D is far out of resonance, still it is affected by the cavity, but does not cross with the isolated A polariton energies. The simulation box is 40.07 Å, with a spacing of 0.397 Å and 6/40 photon number states for many-body/isolated calculations.

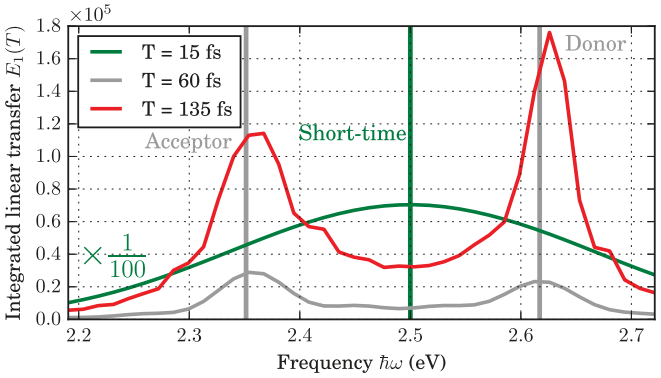

Fig. 8. Integrated first-order excitation energy transfer with interatomic distance 42.3 Å and weak coupling (for the reference frequency $\hbar\omega_{\text{ref}} = 2.340$ *eV* we have $g/\hbar\omega_{\text{ref}} = 0.0058$) for different frequencies and three different integration times $T = \{15, 60, 135\}$ fs. Note that the result for $T = 15$ fs is amplified by a factor of 100. Indicated by vertical lines are the short-time optimal cavity frequency and the A and D isolated excitations. For long coherences, the latter become maxima, and the short-time maximum (equal Hopfield coefficients) becomes a minimum. Notice that the slight detuning from resonance coincides with the many-body–induced energetic shift of Fig. 7. The simulation box is 79.75 Å, with a spacing of 0.397 Å and six photon number states.

Short-Time Configuration. For short coherence times—i.e., in the regime where we assume T of the order of a few femtoseconds—the electronic system has almost no time to explore the space of many-body resonances, and high efficiency is directly connected with short-time maxima.

If we consider weak coupling (see Fig. 8 for details), a very efficient short-time transfer with $T = 15$ fs happens for frequencies which lie in the middle between the isolated excitations of D and A. The most favorable setup ($\hbar\omega \approx 2.5\ eV$) is the one that shows a very fast oscillation (see Fig. 10, where it is visible) when both relative phases—i.e., the energetic difference between lower and middle and middle and upper polariton—are identical.** This result is supported by considering the Hopfield coefficients (see *SI Appendix*, section 3 for more details)—i.e., the relative contribution of the isolated states to the many-body states.

In Fig. 9, we show the Hopfield coefficients for the middle polariton, which is the correlated many-body state that is most dominantly a mixture of D and A. Consequently, the middle polariton is the most essential state for excitation energy transfer between both matter subsystems A and D. At $\hbar\omega \simeq 2.5\ eV$, the D and A contributions become equal, which allows an efficient direct transfer of excitation energy. For strong coupling, this becomes even more efficient since the A and D contributions become larger, while at the same time, the photon contribution becomes very small, which allows the transfer to bypass a strong excitation of the photon field. This observation is in line with few-level calculations in a dephasive two-level Master-equation treatment (8, 9).

Long-Time Configuration. However, in light-harvesting complexes, long coherence times >40 fs are possible (14, 15), leading potentially to coherent dynamics over hundreds of femtoseconds (14). The conditions for efficient excitation energy transfer on such time scales can be very different. To identify these conditions, we investigate in the following three different coherence times $T = \{15, 60, 135\}$ fs, and we consider the weak- and strong-coupling limits. In the weak-coupling situation shown in Fig. 8 [integrated first-order excitation energy transfer $E_1(T)$] and 10 [first- and second-order excitation energy transfer $e_1(t)$ and $e_2(t)$], we observe for long-time propagation distinct peaks. These peaks are close to the isolated A and D lowest excitations.†† This indicates that long-term coherences favor a maximal transfer efficiency around those frequencies, although the isolated energies no longer exist in the many-body spectrum.‡‡

In the strong-coupling limit, where we increase the coupling by a factor of 10 (for the reference frequency $\hbar\omega_{\text{ref}} = 2.340\ eV$, this is $g/\hbar\omega_{\text{ref}} = 0.058$), the excitation energy transfer between the different subsystems is strongly enhanced. Since in this regime the eigenenergies of the isolated systems become completely "dissolved" in the many-body spectrum, we do not find a maximal efficiency at the isolated excitation energies of A and D anymore. Also, while the transfer efficiency was peaked in the weak-coupling regime, now the possible frequency range to have a very effective energy transfer is broadened. The specific maxima, in contrast to the weak coupling situation, depend strongly on the coherence time T, and hence we refrain from showing a dedicated figure. However, these strong-coupling results question the validity of single-mode and few-level approximations, since the interplay of the different energies of matter and photon subsystems is very complex and highly nonlinear processes become important as can already be observed for weak-coupling situations (Fig. 10).

It is important to highlight the relevance of the second-order excitation transfer in the weak-coupling as well as strong-coupling situation, which we use as an indication for nonlinear processes in the excitation transfer. While in the weak-coupling case the nonlinear processes build up over a long coherence time (and can increase far beyond the first-order transfer), in the strong-coupling case this happens very fast. These nonlinear processes strongly depend on the Coulomb interaction and

**The frequency connected to this maximum corresponds to the energetic difference between lower (A) and upper (D) polariton. At this maximum point, the relation between this energy and the competing energies lower-middle and middle-upper polariton reaches its maximum.

††In this case, the corresponding phase associated with the energetic difference between lower/upper and middle polariton becomes minimal, and the amplitude between time-propagated wave function and A/D state is larger. As a result, this configuration dominates on long time scales.

‡‡We note that a slightly higher integrated first-order efficiency at the D resonance prevails also if we reverse the process, i.e., that we consider excitation energy transfer from A to D.

self-polarization term, which are both usually neglected for simple few-level systems. Hence, when the coherence time is large, as in light-harvesting complexes (14), the influence of these terms can become apparent.

To conclude this section about excitation energy transfer, we highlight the difference in short-time vs. long-time behavior. If due to strong system–bath interactions, we only have relatively short coherent dynamics, then a cavity frequency between the isolated D and A resonances leads to a strong energy transfer. For longer times, a cavity with a frequency near the isolated A or D resonances is beneficial. Especially in this latter domain, the influence of the self-polarization and Coulomb interaction as well as higher excited states becomes obvious.

Photon-Induced Correlations

Let us finally return to photon-assisted electron–electron correlations. That photons induce such correlations is not surprising, since it is the (longitudinal) photons that induce the Coulomb interaction among charged particles. A little more interesting is the finding of Equilibrium Long-Range Correlation, where we highlight that also the transversal photons can induce electron–electron correlations. These correlations, however, are very weak compared with the longitudinal correlations. In the time-dependent case, we expect a stronger influence of the transversal photons. Here, we want to quantify their contribution in the afore introduced excitation energy transfer setup 2 (Fig. 2).

To investigate and quantify these photon-induced correlations, we consider besides the electronic 1RDM two further types of reduced density matrices

$$\gamma_{\mathrm{P}}(q,q',t)=\int dx_1\int dx_2\Psi(x_1,x_2,q,t)\Psi^*(x_1,x_2,q',t), \quad [3]$$

$$\Gamma_{\mathrm{e}}(x_1x_2,x_1'x_2',t)=\int dq\Psi(x_1,x_2,q,t)\Psi^*(x_1',x_2',q,t). \quad [4]$$

Again, we choose a normalization of these density matrices to one, such that the following holds

$$tr(|\Psi\rangle\langle\Psi|)=tr_{\mathrm{p}}(\gamma_{\mathrm{P}})tr_{\mathrm{ee}}(\Gamma_{\mathrm{e}})=tr_{\mathrm{p}}(\gamma_{\mathrm{P}})tr_{\mathrm{e}}(\gamma_{\mathrm{e}})tr_{\mathrm{e}}(\gamma_{\mathrm{e}})=1,$$

where the traces run over different (sub)spaces as indicated. Of course, this equality does not hold on the level of density matrices, unless they are completely uncorrelated. In this case, each 1RDM individually should correspond to a pure single-particle state and is consequently idempotent—i.e., their purity $tr_{\mathrm{e/p}}(\gamma^2_{\mathrm{e/p}})$ should be equal to one. If we find a purity that is <1, we have a linear combination of several single-particle states. In the specific case that we start from an equilibrium configuration with essentially only two occupied Slater determinants—i.e., the minimal basis LCAO limit of Equilibrium Long-Range Correlation—then the electronic 1RDM only contains two single-particle states such that the purity is exactly $1/2$. If the purity drops $<1/2$, then we know that we have more than a two-determinant wave function and more single-particle states contribute, we can talk about nontrivial dynamic correlation.

If we plot the purities for weak light–matter coupling (see Fig. 11 for details), we find for $\hbar\omega=2.340\ eV$ that the photonic state is almost the pure vacuum and the dynamical correlation (beyond LCAO correlation) in the electronic coordinates remains small. If we increase the photon occupation by increasing the frequency to $\hbar\omega=2.612\ eV$ (close to resonance with the isolated excitation of D), the photon purity is reduced, as now two states ($|0\rangle_{\mathrm{p}}$, $|1\rangle_{\mathrm{p}}$) are present. We also see that this reduces the electronic purity.

Besides the purity, the light–matter interaction also affects the photonic fluctuations since the interaction with the electrons induces anharmonicities in the photonic system (16, 26). Consequently, the photonic vacuum state is no longer a simple Gaussian, but is elongated along the displacement coordinate $\langle\Delta\hat{q}^2\rangle$ with $\Delta\hat{q}=\hat{q}-\langle\hat{q}\rangle$, $\hat{q}=\sqrt{\frac{\hbar}{2\omega}}\left(\hat{a}+\hat{a}^\dagger\right)$. This elongation $\langle\Delta\hat{q}^2\rangle$ (Fig. 11) is therefore a measure for the nonlinearity of the photonic system due to the presence of matter—i.e., the amount to which photons can interact with each other via a polarizable medium.[§§] The fluctuations increase substantially, even for weak

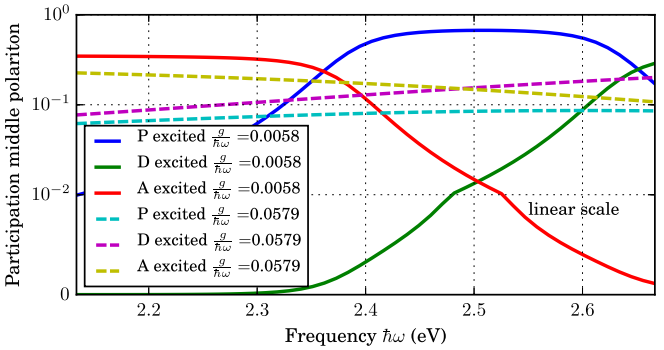

Fig. 9. Hopfield coefficients for the middle polariton with interatomic distance 21.2 Å for different frequencies. The coupling is given with respect to the reference frequency $\hbar\omega_{\mathrm{ref}}=2.340\ eV$. For $\hbar\omega=2.50\ eV$, we observe equal weights of D and A. For weak coupling, the photonic (P) contribution is dominant, while for strong coupling, it is A and D. The equal weight in the middle polariton appears at the short-time excitation-energy-transfer maximum of Fig. 8. The simulation box is 40.07 Å, with a spacing of 0.397 Å and six photon number states.

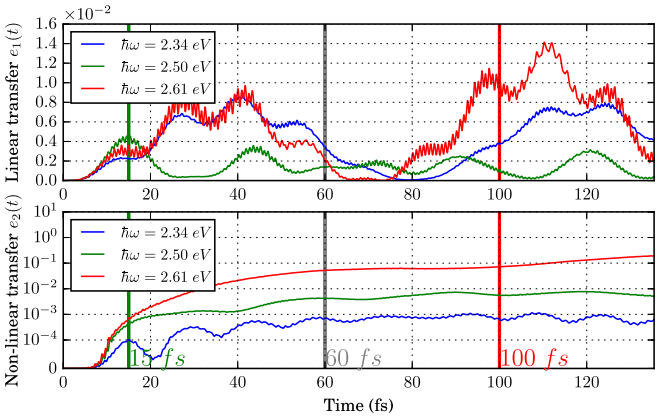

Fig. 10. First-order (*Upper*) and second-order (*Lower*) excitation energy transfer for weak coupling (for the reference frequency $\hbar\omega_{\mathrm{ref}}=2.340\ eV$, this is $g/\hbar\omega_{\mathrm{ref}}=0.0058$) with interatomic distance 42.3 Å. Notice the difference in scales. The relative strength of the second-order excitation energy transfer is very sensitive to the self-polarization and Coulomb interaction. For short times ($t<15$ *fs*), first-order excitation energy transfer is dominant, with an optimal transfer for a cavity frequency in between D and A isolated excitations. Between 15 and 60 *fs*, long-time coherences build up, which lead to the long-time peak structure of Fig. 8 and allow a drastic amplification of second-order excitations. For $t>60$ *fs*, the long-time coherences determine the excitation energy transfer, and the second-order transfer becomes dominant. The simulation box is 79.75 Å, with a spacing of 0.397 Å and six photon number states.

[§§] In reality, as a medium consists of an ensemble of molecules, the induced anharmonicities are influenced also by collective effects of the full ensemble. Furthermore, higher-order perturbative effects can become essential in the thermodynamic limit, which is indeed achievable by modern experimental investigations (27).

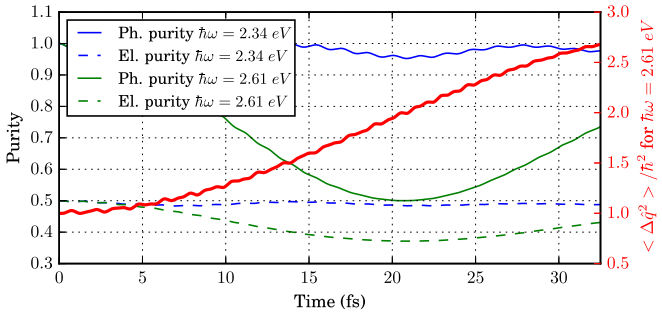

Fig. 11. Photonic (Ph.; solid) and electronic (El.; dashed) purities (left axis) for weak coupling (for reference frequency $\hbar\omega_{\text{ref}} = 2.340\ eV$ that is $g/\hbar\omega_{\text{ref}} = 0.0058$) of setup 2 with interatomic distance 42.3 Å and different frequencies. Both purities follow dominantly the mode occupation. The photonic displacement variance (red, right axis) increases substantially for higher frequency. The simulation box is 79.87 Å, with a spacing of 0.529 Å and six photon number states.

coupling. We note that also the momentum fluctuations $\langle \Delta \hat{p}^2 \rangle$ increase by a similar factor.

Besides the influence of photon-assisted correlations on fundamental quantities such as the photon fluctuations, also the processes itself can be influenced. For this, we rewrite the first-order excitation transfer $e_1(t)$ of Eq. **1** in the following way

$$\begin{aligned} e_1(t) &= tr_{\text{ee}} \left(\sum_{k,n=0}^{N_p} \langle \psi_t^e(0) | \langle k | \Psi(t) \rangle \langle \Psi(t) | n \rangle | \psi_t^e(0) \rangle \right) \\ &\approx tr_{\text{ee}} (\Gamma_{\text{e}} | \psi_1(0) \rangle \langle \psi_1(0) |) \sum_{k,n=0}^{N_p} \langle k | \gamma_{\text{p}} | n \rangle, \end{aligned} \quad \textbf{[5]}$$

where we used that $\hat{\mathbb{1}} = \sum_{n=0}^{N_{\text{p}}} |n\rangle\langle n|$ in our restricted photon space. In the last step, we assumed that electronic and photonic degrees of freedom are uncorrelated—i.e., $\Psi(t)\Psi^*(t) \approx \Gamma_e(t) \otimes \gamma_{\text{p}}(t)$. Physically, we therefore assume that the interaction between electrons and photons is purely classical.

Next, also assuming that the electronic system is uncorrelated, we can factorize the spin-singlet two-body reduced density matrix Γ_{e} by

$$\Gamma_{\text{e}}(x_1 x_2, x_1' x_2', t) \approx \gamma_{\text{e}}(x_1, x_1', t) \gamma_{\text{e}}(x_2, x_2', t).$$

This corresponds to the uncorrelated or mean-field contribution. The linear-order excitation transfer should then approximately be given by

$$e_1^{\text{MF}}(t) = tr_{\text{e}}(\gamma_{\text{e}}(t)\gamma_{\text{e}}^1(0))^2 \sum_{k,n=0}^{N_p} \langle k | \gamma_{\text{p}} | n \rangle, \quad \textbf{[6]}$$

where $\gamma_{\text{e}}^1(0)$ is the electronic 1RDM of $\psi_1(0)$. If we then compare the wave-function–based (WF) transfer $e_1(t)$ and the uncorrelated approximations (see Fig. 12 for details), we find that the process depends strongly on the electronic correlations. While the first approximation of Eq. **5** that treats electrons and photons on a classical mean-field level but keeps all of the electron–electron correlations (also due to the photons) explicit is very accurate, the approximation of Eq. **6** that also treats the electron–electron correlation on mean-field (still the single-electron quantities are exact) is completely wrong. We therefore conclude that Coulombic and photon-assisted electron–electron correlations define the excitation–transfer process.[¶¶]

The photon-assisted correlation channel due to the presence of a cavity in its vacuum state allows us to correlate the electronic system over large distances. We have seen in multiple correlation measures that this is a nonnegligible effect with direct impact on observables such as the linear excitation transfer.

Summary and Conclusion

In this work, we have presented examples of how a change of the electromagnetic vacuum due to a cavity can drastically alter a fundamental chemical process, such as charge and excitation energy transfer. Here a first-principles real-space formulation was advantageous since it allowed us easy access to distance-dependent quantities such as transfer efficiencies that we could compare with the standard quantum-chemical situations for free-space quantum mechanics. Decoherence effects were included effectively by considering only dynamics within a specific coherence-time interval.

We found that a dark cavity can induce electron–electron correlations, which lead to an entanglement of electronic degrees of freedom over large distances and become important, especially in excitation energy transfer. Depending on the coherence times, excitation energy transfer can be enhanced most efficiently by a cavity that has a frequency that is in between the excitations of the isolated donor and acceptor system (short coherence times) or by a cavity that has a frequency in resonance with the isolated excitations of the donor or acceptor system (long coherence times). A slight energetic shift from the exact isolated energies is a consequence of the many-body interaction between D and A electrons and nuclei. In contrast to the usual free-space Förster case, the transversal photons due to a cavity lead to an almost distance-independent excitation energy transfer as well as a drastically enhanced transfer efficiency. The same holds true for charge transfer, where avoided crossings in the many-body spectrum due to the photon degrees of freedom lead to very efficient processes, even when the donor and acceptor are very far apart. This is in contrast to the free-space Dexter transfer, where the efficiency is exponentially suppressed with increasing distance. Many of the observed effects are very sensitive to the Coulomb and self-polarization interactions as well as the chosen coherence times. Our investigations strongly

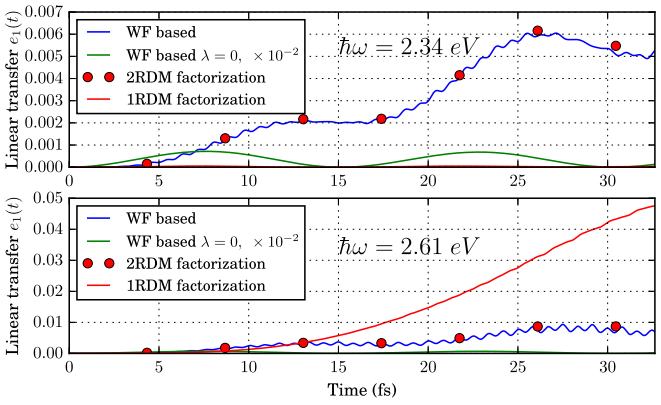

Fig. 12. First-order excitation transfer for setup 2 with interatomic distance 42.3 Å for no (note the factor 100) and weak coupling ($g/\hbar\omega_{\text{ref}} = 0.0058$, $\hbar\omega_{\text{ref}} = 2.340\ eV$) and two different frequencies. We compare the exact wave-function–based (WF) expression of Eq. **1** with the approximations of Eqs. **5** and **6**. For weak coupling, the impact of correlation between electronic and photonic system on the linear excitation transfer remains small for short times, since the classical approximation of Eq. **5** is very accurate. Especially for small photonic occupations ($\hbar\omega = 2.340\ eV$), electronic correlation dominates the transfer, and the mean field is vanishingly small. For the situation of substantial mode occupation ($\hbar\omega = 2.612\ eV$), the mean-field approximation drastically overestimates the transfer. Disregarding electronic correlation results in tremendous deviations. The simulation box is 79.87 Å, with a spacing of 0.529 Å and six photon number states.

[¶¶]We note, that even for strong light–matter coupling, the correlation between photonic and electronic system never reaches the impact of direct electron–electron correlation in our calculations—i.e., the deviation of Eq. **5** is much smaller than of Eq. **6**.

suggest that the theoretical description of chemistry under the influence of a strongly coupled quantized mode demands a consistent first-principles description. Novel techniques such as quantum-electrodynamic density-functional theory (17) and the cavity-Born–Oppenheimer approximation (18) could realize this milestone in the near future, although our results, especially presented in Photon-Induced Correlations, set demanding requirements for those techniques. Many well-established results of molecular physics change under those novel conditions, and control of chemical properties by adopting the photon field seems possible. The present findings could be extended to the cavity-mediated interaction between 2D materials and nanostructures. By selectively addressing single-molecular dimers in specific fixed configurations as, e.g., possible on surfaces (28) or in strongly confined fields (29), the gathered insights could be directly validated in experiment, paving the way to novel technological advances.

Materials and Methods

The electronic structure is calculated on a 2D grid as indicated in the figures, where derivatives are performed by fourth-order finite differences. The photonic contribution is included through a converged truncated expression for the creation and destruction operators with a dimension as indicated. Special caution is demanded for ultrastrong couplings and large dipole moments, as the photonic occupation then rises $\propto (\lambda X)^2$. Further research in this direction could profit from an adjusted basis according to ref. 16. Time propagations use the Lanczos method. We ensured that the results do not change more than a few percent, especially the physical conclusion, for increasing the simulation box or decreasing the spacing. The interatomic distances are selected such that charge and excitation energy transfer are significantly distinct.

ACKNOWLEDGMENTS. We thank Arunangshu Debnath and Johannes Flick for insightful discussions. This work was supported by European Research Council Grant ERC-2015-AdG-694097 and partially supported by Federal Ministry of Education and Research Grant RouTe-13N14839.

1. Ebbesen TW (2016) Hybrid light–matter states in a molecular and material science perspective. *Acc Chem Res* 49:2403–2412.
2. Ruggenthaler M, Tancogne-Dejean N, Flick J, Appel H, Rubio A (2018) From a quantum-electrodynamical light-matter description to novel spectroscopies. *Nat Rev Chem* 2:0118.
3. Hutchison JA, Schwartz T, Genet C, Devaux E, Ebbesen TW (2012) Modifying chemical landscapes by coupling to vacuum fields. *Angew Chem Int Ed* 51:1592–1596.
4. Thomas A, et al. (2016) Ground-state chemical reactivity under vibrational coupling to the vacuum electromagnetic field. *Angew Chem Int Ed* 55:11462–11466.
5. Zhong X, et al. (2016) Non-radiative energy transfer mediated by hybrid light-matter states. *Angew Chem Int Ed* 55:6202–6206.
6. Götzinger S, et al. (2006) Controlled photon transfer between two individual nanoemitters via shared high-Q modes of a microsphere resonator. *Nano Lett* 6:1151–1154.
7. Du et al. (2018) Theory for polariton-assisted remote energy transfer. *Chem Sci* 9:6659–6669.
8. Reitz M, Mineo F, Genes C (2018) Energy transfer and correlations in cavity-embedded donor-acceptor configurations. *Sci Rep* 8:9050.
9. Sáez-Blázquez R, Feist J, Fernández-Domínguez A, García-Vidal F (2018) Organic polaritons enable local vibrations to drive long-range energy transfer. *Phys Rev B* 97:241407.
10. Olaya-Castro A, Scholes GD (2011) Energy transfer from Förster–Dexter theory to quantum coherent light-harvesting. *Int Rev Phys Chem* 30:49–77.
11. Wu P, Brand L (1994) Resonance energy transfer: Methods and applications. *Anal Biochem* 218:1–13.
12. Flick J, Narang P (2018) Cavity-correlated electron-nuclear dynamics from first principles. *Phys Rev Lett* 121:113002.
13. Spohn H (2004) *Dynamics of Charged Particles and Their Radiation Field* (Cambridge Univ Press, Cambridge, UK).
14. Schlau-Cohen GS, et al. (2012) Elucidation of the timescales and origins of quantum electronic coherence in LHCII. *Nat Chem* 4:389–395.
15. Duan HG, et al. (2017) Nature does not rely on long-lived electronic quantum coherence for photosynthetic energy transfer. *Proc Natl Acad Sci USA* 114:8493–8498.
16. Schäfer C, Ruggenthaler M, Rubio A (2018) Ab initio nonrelativistic quantum electrodynamics: Bridging quantum chemistry and quantum optics from weak to strong coupling. *Phys Rev A* 98:043801.
17. Ruggenthaler M, et al. (2014) Quantum-electrodynamical density-functional theory: Bridging quantum optics and electronic-structure theory. *Phys Rev A* 90:012508.
18. Flick J, Ruggenthaler M, Appel H, Rubio A (2017) Atoms and molecules in cavities, from weak to strong coupling in quantum-electrodynamics (QED) chemistry. *Proc Natl Acad Sci USA* 114:3026–3034.
19. De Liberato S (2017) Virtual photons in the ground state of a dissipative system. *Nat Commun* 8:1465.
20. Bhaskara VS, Panigrahi PK (2017) Generalized concurrence measure for faithful quantification of multiparticle pure state entanglement using Lagrange's identity and wedge product. *Quantum Inf Process* 16:118.
21. Flick J, Schäfer C, Ruggenthaler M, Appel H, Rubio A (2017) Ab-initio optimized effective potentials for real molecules in optical cavities: Photon contributions to the molecular ground state. *ACS Photonics* 5:992–1005.
22. Rokaj V, Welakuh D, Ruggenthaler M, Rubio A (2017) Light–matter interaction in the long-wavelength limit: No ground-state without dipole self-energy. *J Phys B At Mol Opt Phys* 51:034005.
23. Craig D, Thirunamachandran T (1998) *Molecular Quantum Electrodynamics: An Introduction to Radiation-Molecule Interactions*, Dover Books on Chemistry Series (Dover Publications, Mineola, NY).
24. Slootsky M, Liu X, Menon VM, Forrest SR (2014) Room temperature Frenkel-Wannier-Mott hybridization of degenerate excitons in a strongly coupled microcavity. *Phys Rev Lett* 112:076401.
25. Yoshihara F, et al. (2017) Superconducting qubit–oscillator circuit beyond the ultrastrong-coupling regime. *Nat Phys* 13:44–47.
26. Hoffmann NM, Appel H, Rubio A, Maitra NT (2018) Light-matter interactions via the exact factorization approach. *Eur Phys J B* 91:180.
27. George J, et al. (2016) Multiple Rabi splittings under ultrastrong vibrational coupling. *Phys Rev Lett* 117:153601.
28. Khajetoorians AA, Heinrich AJ (2016) Toward single-atom memory. *Science* 352:296–297.
29. Benz F, et al. (2016) Single-molecule optomechanics in "picocavities". *Science* 354:726–729.